LCMR1 deficiency exacerbates LPS-induced lung injury in lung-on-a-chip and mouse models

ZHENFEI MO[1,2], CHENGCHENG SU[1,2], JINXIA LIU[1,2], JIABO REN[1,2], LU LIU[3], YUEMING WANG[2], YANQIN LI[2], CHUNSUN LI[2], ZHEN YANG[2], XIUQING MA[4] and LIANGAN CHEN[2]

[1]Medical School of Chinese People's Liberation Army, Chinese People's Liberation Army General Hospital, Beijing 100853, P.R. China; [2]Department of Pulmonary and Critical Care Medicine, The Eighth Medical Centre, Chinese People's Liberation Army General Hospital, Beijing 100853, P.R. China; [3]Department of Nutrition, The First Medical Centre, Chinese People's Liberation Army General Hospital, Beijing 100853, P.R. China; [4]Department of Pulmonary and Critical Care Medicine, The First Medical Centre, Chinese People's Liberation Army General Hospital, Beijing 100853, P.R. China

Received November 15, 2024; Accepted March 12, 2025

DOI: 10.3892/mmr.2025.13554

Abstract. The oncogene lung cancer metastasis-related protein 1 (*LCMR1*) is associated with neoplastic diseases and *LCMR1* conditional knockout affects cell homeostasis. In the present study, the role of *LCMR1* in lipopolysaccharide (LPS)-induced acute lung injury (ALI) was investigated. Firstly, wild-type C57BL/6 mice were used to establish an LPS-induced ALI model via intratracheal injection of LPS, and the expression of LCMR1 was examined at 24, 48, 72 and 96 h after injury. The LPS-induced lung injury model was subsequently constructed in mice with conditional knockout of *LCMR1* in type II alveolar epithelial cells (AEC-II). Subsequently, histopathological analysis, lung wet/dry weight ratio comparisons and lung function tests were performed; survival rates after LPS challenge of the conditional knockout mice were measured; bronchoalveolar lavage fluid (BALF) was collected, and the concentrations of protein and inflammatory cytokines in BALF were measured; and transmission electron microscopy of lung tissue was conducted to evaluate the degree of lung injury. To further investigate the mechanism, a lung-on-a-chip model with overexpression or knockdown of *LCMR1* was constructed to simulate the alveolar environment under LPS treatment. The expression levels of E-cadherin and pro-pulmonary surfactant C precursor (proSP-C) in the chips were determined by immunofluorescence, and the integrity of the air-blood barrier was analyzed using a permeability assay. In the mouse model, LCMR1 expression was downregulated in wild-type mice with LPS-induced lung injury. *LCMR1* conditional knockout in AEC-II caused increased mortality, impaired lung function, aggravated pathological damage and increased the inflammatory response in mice with LPS-induced ALI. Furthermore, in the lung-on-a-chip model, *LCMR1* knockdown reduced the expression of E-cadherin and proSP-C, and impaired the air-blood barrier function, whereas *LCMR1* overexpression attenuated these effects, which may be related to cell differentiation dysfunction and enhanced apoptosis. In conclusion, the present study revealed that *LCMR1* deficiency may exacerbate LPS-induced ALI and could be considered a novel target for intervention in ALI.

Correspondence to: Dr Xiuqing Ma, Department of Pulmonary and Critical Care Medicine, The First Medical Centre, Chinese People's Liberation Army General Hospital, 28 Fuxing Road, Haidian, Beijing 100853, P.R. China
E-mail: mxq820812@163.com

Professor Liangan Chen, Department of Pulmonary and Critical Care Medicine, The Eighth Medical Centre, Chinese People's Liberation Army General Hospital, 28 Fuxing Road, Haidian, Beijing 100853, P.R. China
E-mail: chenliangan301@163.com

Key words: lung cancer metastasis-related protein 1, acute lung injury, lung-on-a-chip, lipopolysaccharide

Introduction

Acute lung injury (ALI), also known as acute respiratory distress syndrome (ARDS), is a complex pathophysiological process characterized by damage to alveolar epithelial cells and vascular endothelial cells resulting from various causes, such as infections, inhalation of toxic chemicals and drowning. This leads to disruption of the pulmonary air-blood barrier function, causing inflammatory cell exudation, pulmonary edema and ultimately respiratory failure (1). The estimated incidence of ARDS can reach 78.9/100000 person-years, and the incidence of hospital admission ranges between 1.3 and 19% worldwide (2). In addition, the in-hospital mortality rate for patients with severe ALI can reach 46.1% (3). Under physiological conditions, endothelial and epithelial cells maintain an air-blood barrier that constitutes the alveoli, preventing the accumulation of fluid or the infiltration of inflammatory cells, such as neutrophils and lymphocytes, into the alveoli, which is also fundamental for maintaining effective gas exchange (4). In the presence of diverse pathological states, such as hypoxia, mechanical strain and bacterial infections, epithelial cells are

damaged. This damage results in the buildup of protein-rich fluid and inflammatory cells within the alveolar spaces (1). Consequently, there is an increase in oxidative stress and the release of inflammatory cytokines, along with impaired gas exchange; this ultimately results in the development of ALI (3-5). Various mechanisms and pathways are involved in the process of ALI, including apoptosis, autophagy, senescence and ferroptosis (6), implicating multiple genes; however, the complexity of this pathophysiological process necessitates further research to elucidate the exact mechanisms.

Previous studies on lung injury have focused on cell and animal models (7-9); however, research at the cellular level cannot reflect the influence of the microenvironment and three-dimensional structure of alveoli (10). Furthermore, studies on animal models typically require the collection of animal specimens for research after modeling, making it impossible to visualize the pathophysiological processes, and animal modeling is time-consuming and expensive (11). Notably, organ-on-a-chip, a new type of *in vitro* model, has attracted attention in recent years; this model integrates tissue engineering and microfluidic technology, which can partially simulate specific tissue microstructures and facilitate the analysis and observation (12). Organ-on-a-chip technology first uses nano-processing methods to fabricate micro-scale chip structures on different substrate materials [such as polydimethylsiloxane (PDMS), polymethyl methacrylate, polypropylene, glass, silicon and paper], and then implants different types of cells or cell clusters wrapped in different materials into the chip microstructure to construct models with different functions. A lung-on-a-chip model approximating an air-blood barrier can be constructed by co-culturing alveolar epithelial cells and vascular endothelial cells on both sides of a porous polymer membrane, which is a suitable model for research on ALI (13). Some researchers have used lung-on-a-chip models to study viral lung infections and drug screening. Notably, there have been reports of simulating rhinovirus, influenza or COVID-19 infections on lung-on-a-chip models, and testing the effects of corresponding drugs; these studies have also identified unique pathways and mechanisms (14-16). However, these studies were all conducted on chips based on regular cell lines, whereas constructing lung-on-a-chip models using gene-edited cell lines and investigating the function of specific genes in disease is a promising direction.

Lung cancer metastasis-related protein 1 (*LCMR1*) is a gene that we previously reported to be highly expressed in non-small cell lung cancer (NSCLC); notably, its expression is highly associated with the stage of NSCLC (17). To further investigate the function of *LCMR1*, a complete *LCMR1* knockout mouse model was generated utilizing CRISPR/Cas9 technology. Our findings indicated that the complete knockout mouse model resulted in homozygous lethality, suggesting that *LCMR1* is indispensable in normal embryonic growth and development (unpublished data). We then established mice with conditional knockout of *LCMR1* in type II alveolar epithelial cells (AEC-II). The results revealed that after AEC-II conditional knockout of the *LCMR1* gene, the mice gradually developed diffuse inflammatory cell infiltration in lung tissue, alveolar hemorrhage, alveolar septal thickening and alveolar edema, which eventually led to respiratory failure and death (18). Previously, research on LCMR1 mainly focused on the field of cancer (19-21); however, based on our previous results, it was hypothesized that the *LCMR1* gene may contribute to the pathogenesis of ALI. To the best of our knowledge, the present study is the first to investigate the role of *LCMR1* in the pathogenesis of ALI on a mouse model of lipopolysaccharide (LPS)-induced ALI. In addition, the underlying mechanism was explored using lung-on-a-chip technology.

Materials and methods

Mouse models. The animal experiments in the present study were approved by the Animal Ethics Committee of Chinese PLA General Hospital (approval no. SQ2023672; Beijing, China) and were carried out in accordance with the ARRIVE 2.0 guidelines (22). All mice were maintained in a specific pathogen-free animal facility with free access to clean food and water at the Laboratory Animal Center of the PLA General Hospital. Mice status was observed every 12 h after LPS administration and assessed according to a murine sepsis score (23), and mice with a score >21 were euthanized and all biological samples were collected for subsequent analyses.

Wild-type male C57BL/6 mice [n=36; age, 8 weeks, weight, 22-24 g, housed under a 12/12 h light/dark cycle in a room with a controlled temperature (23˚C) and humidity (50%)] provided by the Laboratory Animal Center of the PLA General Hospital were used to analyze LCMR1 expression after LPS challenge. The mice were randomly assigned to the LPS group or control group. Anesthesia was induced with 5% isoflurane inhalation and maintained with 2% isoflurane inhalation. Following anesthesia, the mice in the LPS group were intratracheally injected with LPS (10 mg/kg, dissolved in saline, to reach a final concentration of 5 mg/ml LPS; Sigma-Aldrich, cat. no. L2630) to generate an LPS-induced lung injury model, whereas those in the control group were intratracheally injected with saline. After injection, the mice were placed on a vertical operating table and slowly shaken for 1 min to ensure uniform distribution of LPS or saline in the lungs, after which the mice were returned to the animal facility. The lung tissue samples of mice from both groups were collected at 0, 24, 48, 72 and 96 h after LPS/saline injection for histopathological analysis, reverse transcription-quantitative PCR (RT-qPCR) and western blot analysis (n=6 mice/group at 0, 24, 48, 72 and 96 h). Notably, the mice were euthanized by cervical dislocation under anesthesia as aforementioned prior to lung tissue harvest.

Male mice with *LCMR1* conditional knockout in AEC-II were generated based on our previous study (18). Briefly, mice with insertion of the Cre recombinase genes at the pulmonary surfactant protein C (*Sftpc*) locus ($Sftpc^{CreERT2}$ mice) based on C57BL/6 mice (Purchased from Cyagen Biosciences, Inc.) and mice carrying the floxed *LCMR1* allele ($LCMR1^{flox/flox}$ mice, Purchased from Cyagen Biosciences, Inc.) were used. The $Sftpc^{CreERT2}$ mice have a tamoxifen-inducible Cre recombinase controlled by the *Sftpc* promoter that specifically mediates the knockout of target sequences located between *Lox*P sites in AEC-II. $Sftpc^{CreERT2}$; $LCMR1^{flox/flox}$ (*LCMR1*-CKO) mice were generated by crossing $Sftpc^{CreERT2}$ mice with $LCMR1^{flox/flox}$ mice, and the $LCMR1^{flox/flox}$ littermates were used as controls (*LCMR1*-C). A total of 6 $Sftpc^{CreERT2}$ and 6 $LCMR1^{flox/flox}$ mice (weight, 23-25 g) were use as breeding pairs and housed under

a 12/12 h light/dark cycle in a room with a controlled temperature (23˚C) and humidity (50%) provided by the Laboratory Animal Center of the PLA General Hospital.

To induce AEC-II specific deletion of *LCMR1*, tamoxifen (50 mg/kg; Sigma-Aldrich) was dissolved in corn oil (Shanghai Aladdin Biochemical Technology Co., Ltd.) and injected intraperitoneally into mice for 5 consecutive days. Following tamoxifen injection, both the *LCMR1*-C group and the *LCMR1*-CKO group were intratracheally administered LPS (10 mg/kg) to generate an LPS-induced lung injury model, or with sterile saline to serve as a control group. A total of 48 h after LPS/saline administration, the mice (age, 8-10 weeks) were anesthetized as aforementioned and subjected to pulmonary function testing, after which the mice were euthanized by cervical dislocation. The right lung of the mice was harvested and frozen in liquid nitrogen, before being maintained at -80˚C for further biochemical measurements. The left lungs were harvested and stored in 4% paraformaldehyde (PFA) for 24 h at 4°C, for subsequent histological analysis. Each group contained 30 mice, among them, 6 were used for survival analysis after LPS stimulation, 12 were used for pulmonary function testing followed with histological analysis, lung wet/dry weight ratio analysis and transmission electron microscopy (6 with LPS administration and 6 with saline administration), and 12 were used for bronchoalveolar lavage fluid (BALF) analysis (6 with LPS administration and 6 with saline administration). All mice were housed in a specific pathogen-free animal facility with free access to clean food and water at the Laboratory Animal Center of the PLA General Hospital.

Survival analysis. The mice in the *LCMR1*-C and *LCMR1*-CKO groups (n=6/group) were used to analyze the effect of *LCMR1* knockout on the survival of the mice after LPS stimulation. The number of deaths was counted every 24 h and the percentage of survival was calculated. At 120 h, the remaining mice were euthanized under anesthesia by cervical dislocation.

Genotyping. To genotype *LCMR1*-C and *LCMR1*-CKO mice, the mouse tails were snipped between 9 and 14 days of age, after which the mice were housed until 8-10 weeks of age for subsequent experiments. The genomic DNA was extracted from the tails of mice utilizing the Mouse Quick Genotyping Kit (YangGuangBio, cat. no. C190801). The genotype was determined by PCR employing the primers listed in Table SI. PCR amplification was carried out using Premix Taq (Takara, cat. no. RR902A) on the T100™ thermocycler (Bio-Rad Laboratories, Inc.; Table SII. The resultant PCR products were analyzed via agarose gel (1.5%) electrophoresis. For visualization, the ChemiDoc XR imaging system (Bio-Rad Laboratories, Inc.) and Image Lab version 3.0 (Bio-Rad) was utilized.

Lung function testing. Lung function assessment was conducted utilizing the AniRes2005 lung function testing apparatus (Best Lab International, Inc.). Briefly, the process involved anesthetizing the mice, performing a tracheotomy for cannulation and subsequently placing them into a sealed plethysmograph chamber. The mice were then linked to a ventilator through the tracheal cannula. The indices used to evaluate the lung function of mice included forced vital capacity (FVC), proportion of FVC expired in the first second, static lung compliance and lung resistance (24,25). Each mouse was measured five times and the mean value of these indices was recorded.

Histopathological analysis. Lung tissues from mice were preserved in 4% paraformaldehyde (PFA) for 24 h at 4˚C for fixation. After fixation, the tissue samples were dehydrated and embed in wax and then sliced to a thickness of 4 μm. The tissue sections were stained with hematoxylin solution for 3-5 min at room temperature and then stained with Eosin dye for 15 sec at room temperature. The stained tissue sections were analyzed using a NanoZoomer system (Hamamatsu Photonics K.K.). The assessment of lung injury severity was performed by two pathologists, who were unaware of the specifics of the study, employing a previously established scoring system (26).

Lung wet/dry weight ratio. The right lung of the mice was excised and weighed to ascertain the wet weight. Subsequently, the samples underwent desiccation in an oven maintained at 65˚C for 120 h, after which they were weighed again to acquire the dry weight data. Subsequently, the wet/dry weight ratio of the lungs was computed.

Bronchoalveolar lavage fluid (BALF) analysis. Following anesthesia, the mice underwent intubation, and the BALF was collected by three consecutive infusions and withdrawal of 1-ml PBS into the tracheal cannula. The BALF was centrifuged at 1,500 × g) for 10 min at 4˚C. The resultant supernatant was utilized to quantify total protein concentrations employing the BCA Protein Assay kit (YangGuangBio), whereas inflammatory cytokine levels were assessed utilizing the LEGENDplex Mouse Inflammation Panel (cat. no. 740446; BioLegend, Inc.) according to the manufacturer's protocol.

Transmission electron microscopy. Harvested mouse lung tissues were cut into tissue blocks with a size of no more than 1 mm^3. The tissue blocks were then fixed in 2.5% glutaraldehyde at 4˚C overnight. The specimens were subsequently fixed in a 1% OsO_4 solution within 0.1 M PBS (pH 7.4) for 2 h at room temperature. Following fixation, the samples underwent dehydration through a sequential ethanol concentration and were ultimately embedded in epoxy resin at room temperature for 3 h. Ultrathin sections, measuring 70 nm, were then prepared utilizing an Ultracut E ultramicrotome (Leica Microsystems GmbH) and were stained with a saturated alcoholic solution of 2% uranium acetate for 8 min at room temperature. The prepared sections were later analyzed using an HT7800 transmission electron microscope (Hitachi, Ltd.).

Cell culture and chip fabrication. The human alveolar lung-on-a-chip device was kindly provided by Professor Jianhua Qin (Division of Biotechnology, Chinese Academy of Science Key Laboratory of separation science for analytical chemistry, Dalian Institute of Chemical Physics, Chinese Academy of Sciences, Dalian, China). This device mainly consists of two channels made by casting a PDMS prepolymer on a mold fabricated by a conventional soft lithography process (27). The device was sterilized in an autoclave, and transferred to an ultraclean table under UV light overnight.

Both sides of the porous part of the device were covered with 200 μg/ml type I rat tail collagen (diluted at a 1:100 ratio with glacial acetic acid; Corning, Inc.) for 48 h at room temperature before cell seeding.

The human AEC-II line (HPAEpiC; passage 4) and the vascular endothelial cell line (Hulec-5A) derived from human alveolar epithelial cells were also provided by Professor Jianhua Qin. The HPAEpic cell line was maintained in RPMI 1640 medium (cat. no. 12633020) supplemented with 10% FBS (cat. no. A5256701; both Gibco, Thermo Fisher Scientific, Inc.). Hulec-5A cell line was maintained in dedicated growth medium (cat. no. CM-0565; Procell Life Science & Technology Co., Ltd.). All cells were cultured at 37˚C with 5% CO_2. To construct the lung-on-a-chip model, Hulec-5A and HPAEpiC cells (~1x10^5 cells) were seeded on the bottom and upper channel of the aforementioned chip device, respectively. After cell attachment, a constant flow of medium (50 μl/h) was applied to both layers via a peristaltic pump. The cells were cultured for 3 days until they reached 100% confluence, and the chips were maintained in an incubator at 37˚C with 5% CO_2.

The *LCMR1*-knockdown (*LCMR1*-KD) HPAEpic cell lines were established by lentiviral vector transfection. The vector was generated in cooperation with Vigen Biotechnology Co., Ltd. The short hairpin RNA (shRNA) sequences of the LCMR1 protein and negative control (NC) were designed and synthesized by Vigen Inc. The shRNA sequence and information regarding the lentiviral vector are detailed in Table SIII and Fig. S1. The lentivirus was generated using 2nd generation lentivirus packaging plasmids by co-transfection of psPAX2 (3 μg), pMD2G (1 μg) and pLKO.1 (Addgene Inc.)-shRNA (4 μg) or pLKO.1-shNC (4 μg) into HEK-293T cells (Vigen Biotechnology Co., Ltd, Zhenjiang, China). The 293T cells were further cultured at 37°C for 48 h. Then, the supernatants of HEK-293T cells were collected and concentrated by pEGit (Vigen Biotechnology Co., Ltd, Zhenjiang, China). The *LCMR1*-overexpressing (*LCMR1*-OE) HPAEpiC cells were established by lentiviral vector transfection. Lentivirus was generated by co-transfection of psPAX2 (3 μg), pMD2G (1 μg) and pCDH-CMV-LCMR1(h)-EF1a-Puro (5 μg) or pCDH-MCS-EF1a-Puro (served as NC) into HEK-293T cells (Vigen Biotechnology Co., Ltd, Zhenjiang, China). The 293T cells were further cultured at 37˚C for 48 h. Then, the supernatants of HEK-293T cells were collected and concentrated by pEGit (Vigen Biotechnology Co., Ltd.). The information regarding the lentiviral vector was detailed in Table SIV and Fig. S2.

To generate the *LCMR1*-KD and *LCMR1*-OE HPAEpic cell lines, the HPAEpic cells were placed in 6-well plate, cultivated until reaching a 70-80% density, and exposed to the corresponding lentivirus with 8 μg/ml polybrene (Sigma-Aldrich) with a multiplicity of infection (MOI) of 20 for 48 h at 37°C. Stably transfected cell lines were selected using puromycin. The concentration of selection was 2.5 μg/ml and maintenance concentration were 0.4 μg/ml. After 10 days of puromycin selection, the cells were used for subsequent experimentation. The overexpression and knockdown efficiency of the target protein was evaluated by western blotting, and cell proliferation rate after transfection was detected using the Cell Counting Kit (CCK)8 assay (cat. no. C0038; Beyotime Biotechnology) according to the manufacturer's instruction.

To simulate ALI, LPS (1 μg/ml) was added for 72 h at 37˚C. After which, the media in the alveolar channel were collected from each chip. The concentrations of IL-6 and TNF-α were measured using the LEGENDplex Human Inflammation Panel 1 (Biolegend, USA) according to the manufacturer's instructions.

Immunofluorescence. For immunofluorescence imaging of the chips, the cells were rinsed with PBS through the upper and lower channels, and fixed with 4% PFA at room temperature for 20 min. The cells were then infiltrated with 0.2% Triton X-100 in PBS (PBST) buffer for 5 min and blocked with PBST buffer containing 5% goat serum (cat. no. 16210064, Gibco, Thermo Fisher Scientific, Inc.) for 30 min at room temperature. They were subsequently stained with the corresponding primary antibody overnight at 4˚C and then with the secondary antibody for 1 h at room temperature. After secondary antibody staining, DAPI was used to stain the cell nucleus for 5 min at room temperature. Imaging was carried out using a confocal fluorescence microscope system (LSM880; Carl Zeiss AG), and image analysis was conducted employing Imaris software (Oxford Instruments, version 10.2.0) along with ImageJ (National Institutes of Health, version 1.54 g).

The primary antibodies used were as follows: Anti-E-cadherin (cat. no. 60335-1-Ig; Proteintech Group, Inc. 1:100), anti-VE-cadherin (cat. no. 14-1449-82; Invitrogen; Thermo Fisher Scientific, Inc. 1:100) and anti-pro-pulmonary surfactant C precursor (proSP-C; cat. no. AB3786; MilliporeSigma 1:100). The secondary antibodies were goat anti-mouse IgG (H+L) Cross-Adsorbed Secondary Antibody, Alexa Fluor™ 647 (cat. no. AB_2535804, Invitrogen; Thermo Fisher Scientific, Inc.; 1:1,000), goat anti-mouse IgG (H+L) Cross-Adsorbed Secondary Antibody, Alexa Fluor™ 488 (cat. no. AB_2534069, Invitrogen; Thermo Fisher Scientific, Inc. 1:1,000) and goat anti-Rabbit IgG (H+L) Highly Cross-Adsorbed Secondary Antibody, Alexa Fluor™ Plus 647 (cat. no. A32733, Invitrogen; Thermo Fisher Scientific, Inc. 1:1,000).

Permeability assay. Culture medium containing FITC-dextran (1 mg/ml; MilliporeSigma) was added to the bottom channel of the lung-on-a-chip model after LPS stimulation for 72 h. Subsequently, media were collected from the bottom and upper channels at different time points (0, 1 and 2 h). The fluorescence intensity of the media collected from the upper and bottom channels was measured with a microplate system (Spark®, Tecan Inc.), and the permeability of the air-blood barrier of the chips was evaluated based on their fluorescence intensity ratio.

RT-qPCR. Total RNA was extracted from cells or mouse tissue samples using the Total RNA Kit (cat. no. DP451; Tiangen Biotech Co., Ltd.) according to the manufacturer's instructions. The RNA was then reverse-transcribed to cDNA using the PrimeScript RT reagent Kit with a gDNA Eraser (cat. no. RR047A, Takara) according to the manufacturer's instructions. qPCR was performed using KAPA SYBR FAST Universal (cat. no. KK4601; KAPA Biosystems; Roche Diagnostics). Primer sequences are detailed in Table SI. The thermocycling conditions are listed in Table SV. The standard $2^{-\Delta\Delta Cq}$ assay was applied to calculate the mRNA expression levels relative to *β-actin* (28).

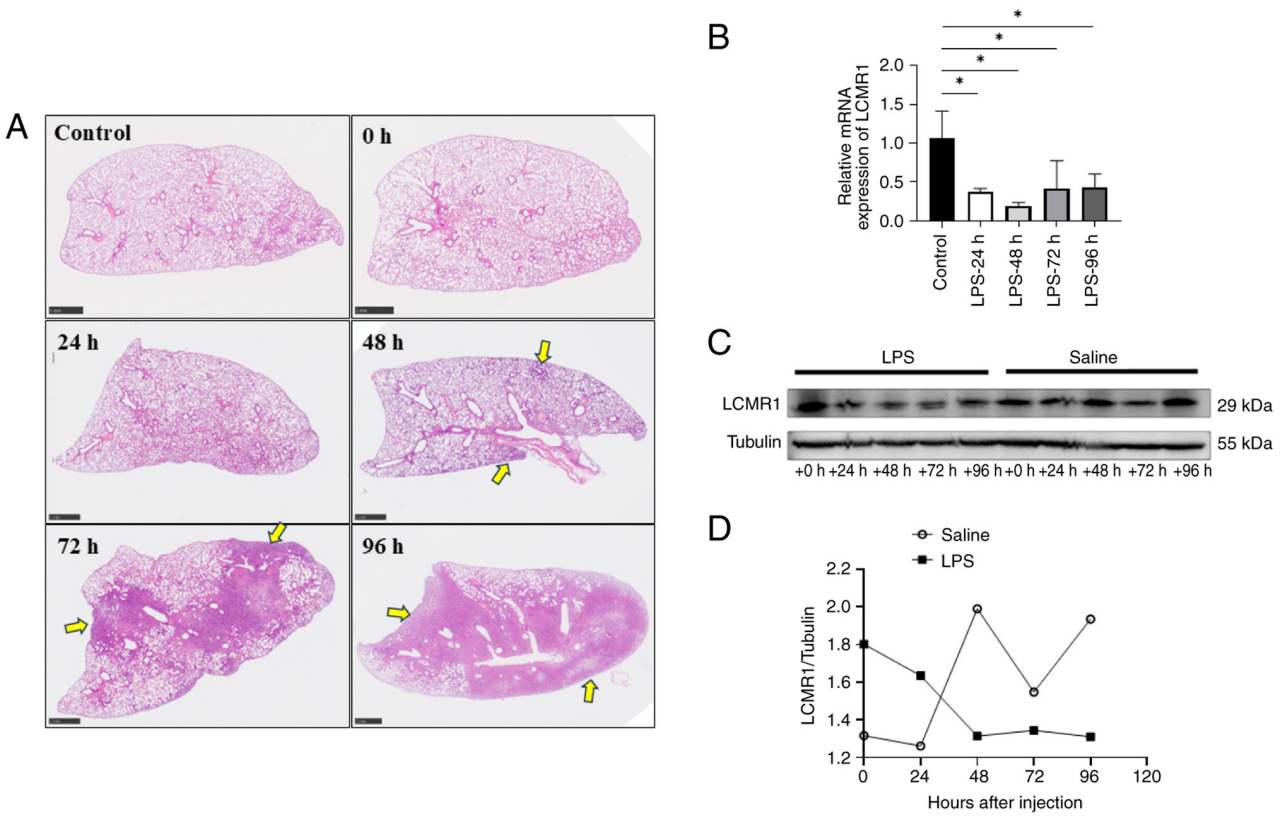

Figure 1. Decreased expression of LCMR1 in wild-type mice with LPS-induced lung injury. (A) Representative pathological images of the left lung of C57BL/6 mice at different time points after LPS challenge (stained with hematoxylin and eosin; scale bar, 1 mm. Arrow indicates changes after LPS stimulation). (B) Reverse transcription-quantitative PCR analysis of *LCMR1* mRNA expression at different times after LPS injection, normalized to *β-actin* (n=6/group at 24, 48, 72 and 96 h after LPS administration). (C) Western blot image of the LCMR1 protein in wild-type C57BL/6 mice at different time points after intratracheal injection of LPS or saline (n=6/group at 0, 24, 48, 72 and 96 h after LPS administration). (D) Gray-scale analysis of western blotting results. (B) Data were analyzed using one-way analysis of variance followed by Tukey's post hoc test. *P<0.05. LCMR1, lung cancer metastasis-related protein 1; LPS, lipopolysaccharide.

Western blotting. Protein was extracted from mouse lung tissue or cells using RIPA) lysis buffer supplemented with protease and phosphatase inhibitor cocktails (cat. no. C1055, Applygen Technologies Inc.). Protein concentration was determined with a bicinchoninic acid protein assay kit and was then separated by gel (12%) electrophoresis with 50 μg protein loaded per lane and transferred to a 0.2-μm nitrocellulose membrane (Cytiva). The membranes were blocked with Tris-buffered saline-0.05% Tween-20 and 5% bovine serum albumin (cat. no. A8020, Solarbio) for 2 h at room temperature and then probed with primary antibodies overnight at 4˚C. The membranes were then probed with a horseradish peroxidase-labeled secondary antibody for 60 min at room temperature. Protein bands were visualized using an automated chemiluminescence imaging system (Tanon Science and Technology Co., Ltd.). The gray values of the bands were then semi-quantified using ImageJ software (version 1.54g). The primary antibodies used were as follows: Anti-tubulin (1:5,000; cat. no. 11224-1-AP; Proteintech Group, Inc.) used as loading control, anti-LCMR1 (1:1,000; cat. no. PA5-44383; Invitrogen; Thermo Fisher Scientific, Inc.), aquaporin 5 (AQP5; 1:1,000; cat. no. 20334-1-AP; Proteintech Group, Inc.), anti-Bcl-2 (1:3,000; cat. no. 12789-1-AP; Proteintech Group, Inc.), anti-Bax (1:3,000; cat. no. ab32503; Abcam) and cleaved caspase-3 (1:5,000; cat. no. ab214430; Abcam). The secondary antibody was HRP-Goat Anti-Rabbit IgG (H&L; 1:3,000; cat. no. C081802; YangGuangBio).

Statistical analysis. No specific statistical test was used to predetermine the sample size. For group comparisons, GraphPad Prism 8 software (Dotmatics) was utilized. The data that conformed to a normal distribution are presented as the mean ± SD. One-way analysis of variance followed by Tukey's post hoc test, or two-way analysis of variance followed by Sidak's post hoc test was applied for statistical comparisons among three or more groups. Unpaired Student's t-test was applied for statistical comparisons between two groups. Data that did not conform to normal distribution are presented as the median (range), and were compared using the Kruskal-Wallis test followed by Dunn's post hoc test. Kaplan-Meier analysis followed by Mantel-Cox test was used for survival analysis. Two-sided P<0.05 was considered to indicate a statistically significant difference.

Results

LCMR1 expression is downregulated in wild-type mice with LPS-induced lung injury. To investigate whether *LCMR1* was associated with LPS-induced ALI in animal models, the protein and mRNA expression levels of LCMR1 were assessed in lung tissues from LPS (10 mg/kg)-treated mice at different time points. Briefly, 8-week-old male wild-type C57BL/6 mice were intratracheally administered LPS (10 mg/kg) to generate an LPS-induced lung injury model. The lung tissue

samples were collected at 24, 48, 72 and 96 h after LPS injury for histopathological, RT-qPCR and western blot analysis. The pathological results showed that there was obvious fluid exudation, inflammatory cell infiltration, alveolar hemorrhage and consolidation in the lungs within 48-96 h of LPS stimulation (Fig. 1A). Notably, the mRNA expression levels of *LCMR1* at 24-96 h after LPS stimulation were downregulated compared with those in the control group, and the protein expression levels of LCMR1 were downregulated 48 h post-LPS stimulation (Fig. 1B-D). The expression of LCMR1 reached its lowest point at ~48 h after LPS challenge; therefore, the intervention time of LPS was set to 48 h in subsequent experiments.

LCMR1 conditional knockout in AEC-II exacerbates LPS-induced ALI in mice. The method used to generate tamoxifen-induced *LCMR1* conditional knockout in AEC-II of mice was described in our previous study (18). The modeling pattern is shown in Fig. 2A. Subsequently, the *LCMR1*-CKO and *LCMR1*-C mice were genotyped; *LCMR1*-CKO mice were carrying the *Sftpc-CreERT2* transgene (210bp; Fig. 2B. After 5 consecutive days of intraperitoneal injection with tamoxifen to induce gene knockout in *LCMR1*-CKO mice, western blot analysis revealed that LCMR1 protein expression was significantly lower in the *LCMR1*-CKO group than that in the *LCMR1*-C group (Fig. 2D). These results indicated the successful knockout of *LCMR1* in AEC-II.

After 5 consecutive days of intraperitoneal injection with tamoxifen, the mice were administered LPS (10 mg/kg) intratracheally. Survival analysis showed that the mortality rate of *LCMR1*-CKO mice was significantly increased after LPS stimulation compared with that in *LCMR1*-C mice (Fig. 2E). Lung function tests revealed that *LCMR1*-CKO mice had decreased FVC, decreased lung compliance and increased lung resistance after LPS-induced lung injury compared with the *LCMR1*-C mice (Fig. 2F-I).

A total of 48 h after LPS stimulation, the mice lungs were harvested. The *LCMR1*-CKO mice showed a more severe lung injury after LPS challenge; macroscopically, the lung of *LCMR1*-CKO mice showed obvious exudation and an overall dark red color (Fig. 2C). The lung pathology revealed that the *LCMR1*-CKO mice presented more severe lung injury manifestations, such as hemorrhage and exudation, than *LCMR1*-C mice after LPS stimulation, whereas *LCMR1*-CKO mice administered with saline also developed localized lesions similar to *LCMR1*-C mice challenged with LPS (Fig. 2J). These findings were confirmed by subsequent lung injury score analysis based on the pathology images (Figs. 2J and 3B). Furthermore, the *LCMR1*-CKO mice had increased wet/dry weight ratios (Fig. 3A) and increased levels of inflammatory cytokines in the BALF (Fig. 3C-F) compared with *LCMR1*-C mice following LPS stimulation. Among the inflammatory cytokines, IL-1β, IL-6 and TNF-α were significantly increased in *LCMR1*-CKO mice comparing to *LCMR1*-C mice, and the protein content in the BALF of *LCMR1*-CKO mice was also increased comparing to *LCMR1*-C mice. Western blot analysis revealed that *LCMR1* knockout significantly increased the Bax/Bcl-2 protein ratio (Fig. 3G and H) and cleaved caspase-3/caspase-3 protein ratio (Fig. 3I and J) comparing to *LCMR1*-C mice, indicating enhanced apoptosis.

The present study further examined the alveolar microstructure using transmission electron microscopy (Fig. 4). After *LCMR1* conditional knockout, the AEC-II cells of *LCMR1*-CKO mice were swollen and the number of lamellar bodies was reduced. After LPS stimulation, compared with the *LCMR1*-C mice, the AEC-II cells of *LCMR1*-CKO mice shrank, and the lamellar bodies disappeared indicating a lack of lung alveolar surfactant. The air-blood barrier of was structurally disordered, and the barrier becomes thinner after LPS-induced lung injury.

Generation of lung-on-a-chip model. To further investigate the mechanism by which *LCMR1* deficiency aggravates lung injury, lung-on-a-chip technology was used to simulate the alveolar environment under LPS-induced ALI. First, *LCMR1*-OE and *LCMR1*-KD cells, based on the HPAEpiC cell line, were generated. The expression of LCMR1 was upregulated in *LCMR1*-OE cells comparing to negative controls and was downregulated in *LCMR1*-KD cells comparing to negative controls, verified by RT-qPCR and western blotting (Fig. 5A and B). In addition, the proliferation rate of the gene-edited cells was examined using the CCK8 assay, and the results revealed that the proliferation rate of the *LCMR1*-OE cells increased, whereas that of the *LCMR1*-KD cells decreased comparing to the wild-type HPAEpic cells. (Fig. 5C).

The lung-on-a-chip model used in the present study was constructed according to the method described by Zhang *et al* (27). Immunofluorescence demonstrated that epithelial cells were capable of establishing adhesion junctions characterized by the presence of E-cadherin, whereas endothelial cells were shown to form junctions identified by VE-cadherin. These two types of cells successfully formed an air-blood barrier on the chip device (Fig. 5D-F).

Knockdown of LCMR1 impairs the structure and function of the air-blood barrier. By adding LPS (1 μg/ml) to the flow medium, the microenviroument of alveoli under LPS-induced lung injury was mimicked, and the results revealed that E-cadherin expression was attenuated in *LCMR1*-KD chips after 72 h compared with HPAEpic chips; however, the E-cadherin expression of *LCMR1*-OE group was significantly upregelated comparing to the HPAEpic chips. (Fig. 6A and C). In addition, proSP-C, an important synthetic substance of AEC-II to maintain the homeostasis of the alveolar microenvironment, was detected. The results showed that knockdown of *LCMR1* reduced proSP-C synthesis comparing to *LCMR1*-OE group after LPS stimulation while the *LCMR1*-OE group showed no significant difference in proSP-C synthesis with the HPAEpic group after LPS stimulation (Fig. 6B and D). These findings suggested that *LCMR1* knockdown impaired the epithelial barrier function. Therefore, FITC-glucan was administered to the bottom channal of vascular cells to assess the integrity of the air-blood barrier by comparing the fluorescence intensity of the two channels. The results revealed increased permeability in the *LCMR1*-KD comparing to the HPAEpic group, suggesting impaired barrier integrity (Fig. 6E), while the fluorescence intensity ratio of *LCMR1*-OE group showed no significant change comparing to the HPAEpic group (Fig. 6E). The current study also examined the inflammatory cytokines in the supernatant from the

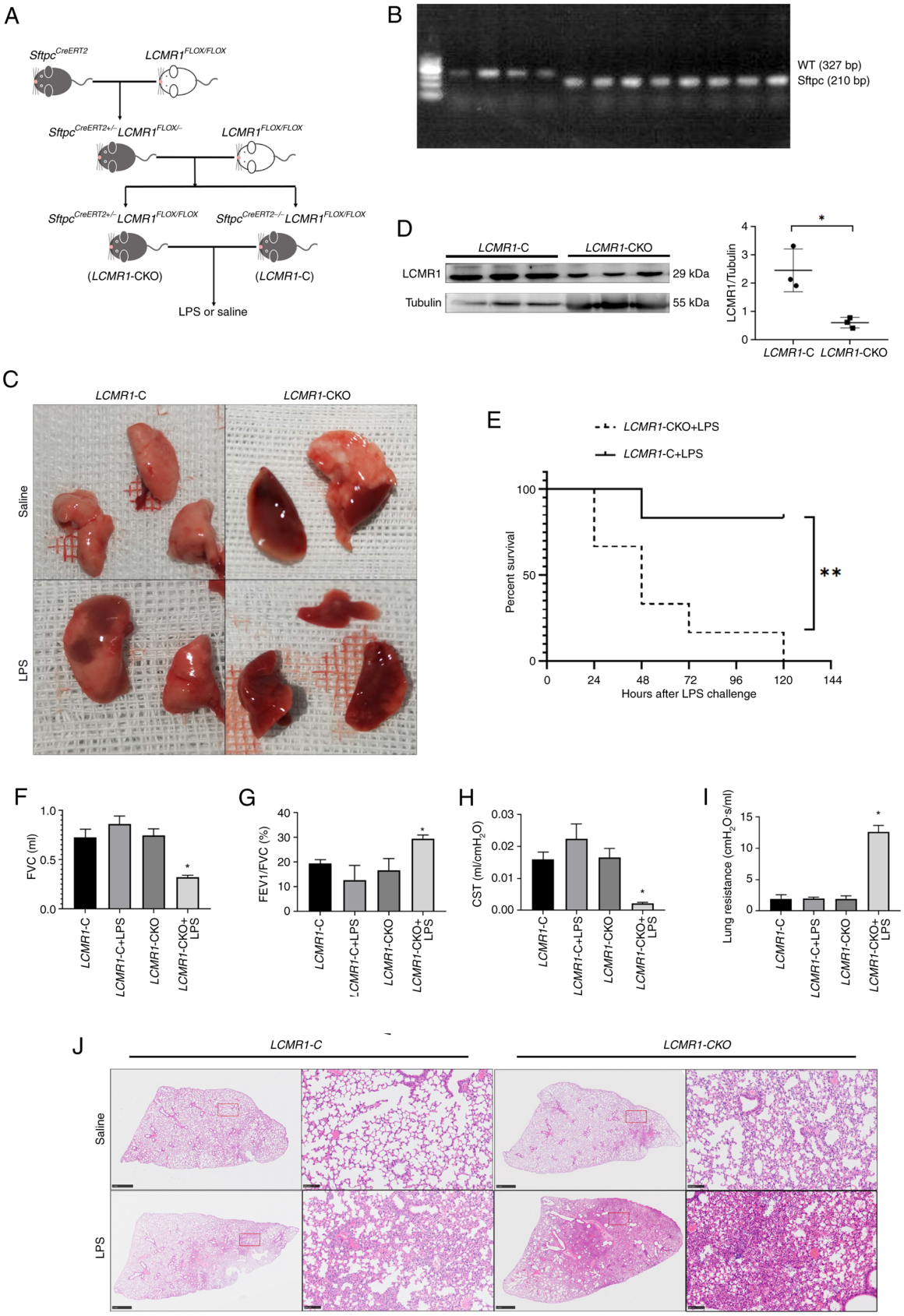

Figure 2. *LCMR1* deficiency in type II alveolar epithelial cells exacerbates LPS-induced lung injury in mice. (A) Schematic diagram of mouse model construction. (B) Genotyping of mice by PCR for the presence of the *Sftpc*^{CreERT2} transgene. (C) Lung tissue harvested 48 h after LPS stimulation. (D) Western blot analysis of LCMR1 protein in lung tissue after tamoxifen administration (n=3/group) (E) Kaplan-Meier survival curve of mice after LPS stimulation. (F-I) Lung function test results, including (F) forced vital capacity, (G) proportion of forced expiratory volume in 1 sec in forced vital capacity, (H) static lung compliance and (I) lung resistance (n=6/group). (J) Representative hematoxylin and eosin staining of the left lung of *LCMR1*-C and *LCMR1*-CKO mice. scale bar on the overall view: 1 mm, scale bar on the magnified view: 100 μm. *P<0.05, **P<0.001. C, control; CKO, conditional knockout; CST, static lung compliance; FEV1, forced expiratory volume in 1 sec; FVC, forced vital capacity; LCMR1, lung cancer metastasis-related protein 1; LPS, lipopolysaccharide; WT, wild-type.

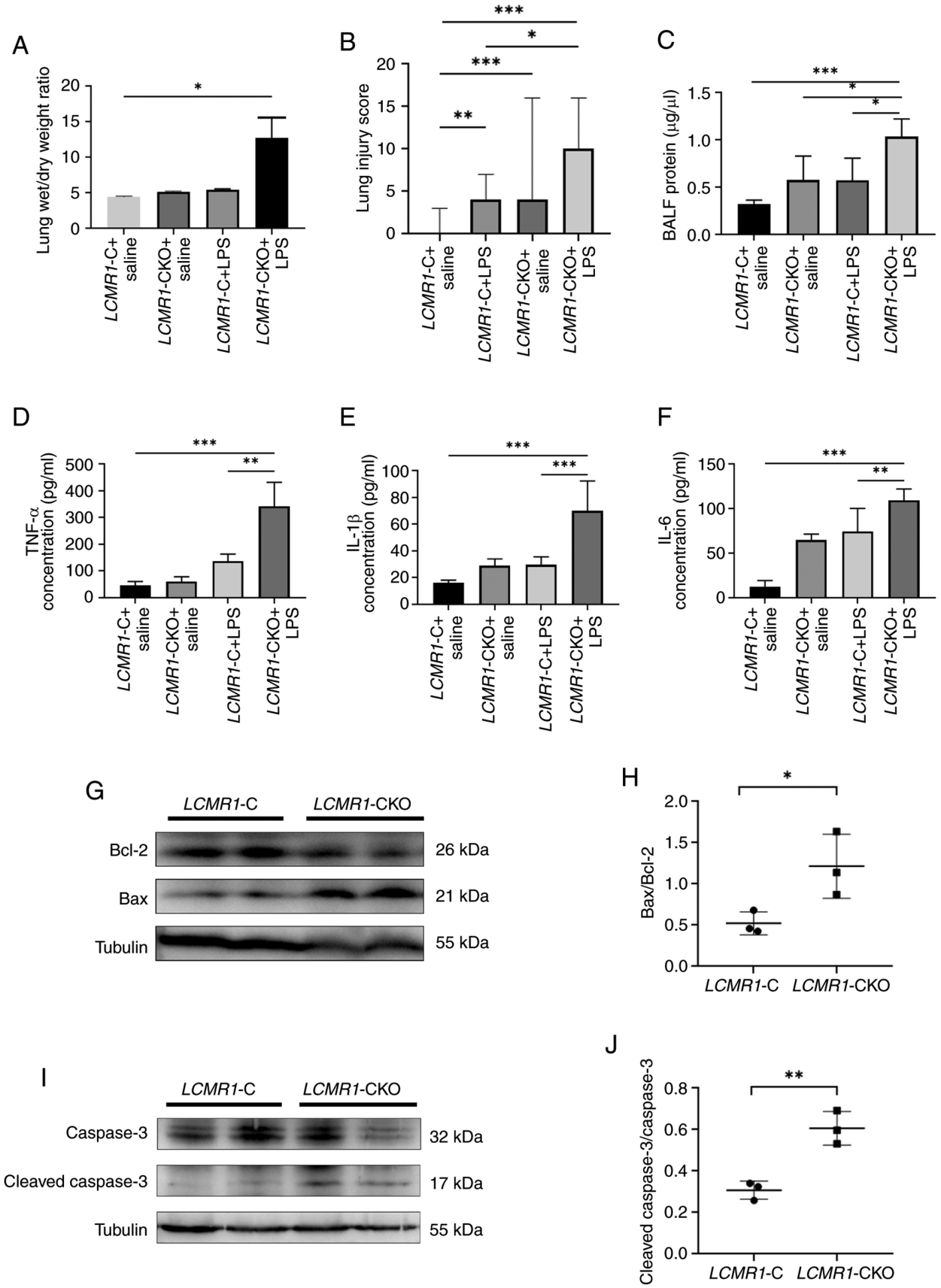

Figure 3. *LCMR1*-CKO mice present with more severe pathological damage, inflammatory response and enhanced apoptosis after LPS-induced lung injury. (A) Mouse right lungs were collected for measurement of wet/dry weight ratio. (B) Lung pathological damage severity was accessed using lung injury scores. BALF was collected and the concentration of (C) total protein, (D) TNF-α, (E) IL-1β and (F) IL-6 in the BALF 48 h after LPS administration were measured (n=6/group). (G) Western blot images of Bax and Bcl-2 protein in murine lung tissues, and (H) statistical results of Bax/Bcl-2 ratio (n=3/group). (I) Western blot images of cleaved caspase-3 and caspase-3 protein in murine lung tissues, and (J) statistical results of cleaved caspase-3/caspase-3 ratio (n=6). *P<0.05, **P<0.001, ***P<0.0001. BALF, bronchoalveolar lavage fluid; C, control; CKO, conditional knockout; LCMR1, lung cancer metastasis-related protein 1; LPS, lipopolysaccharide.

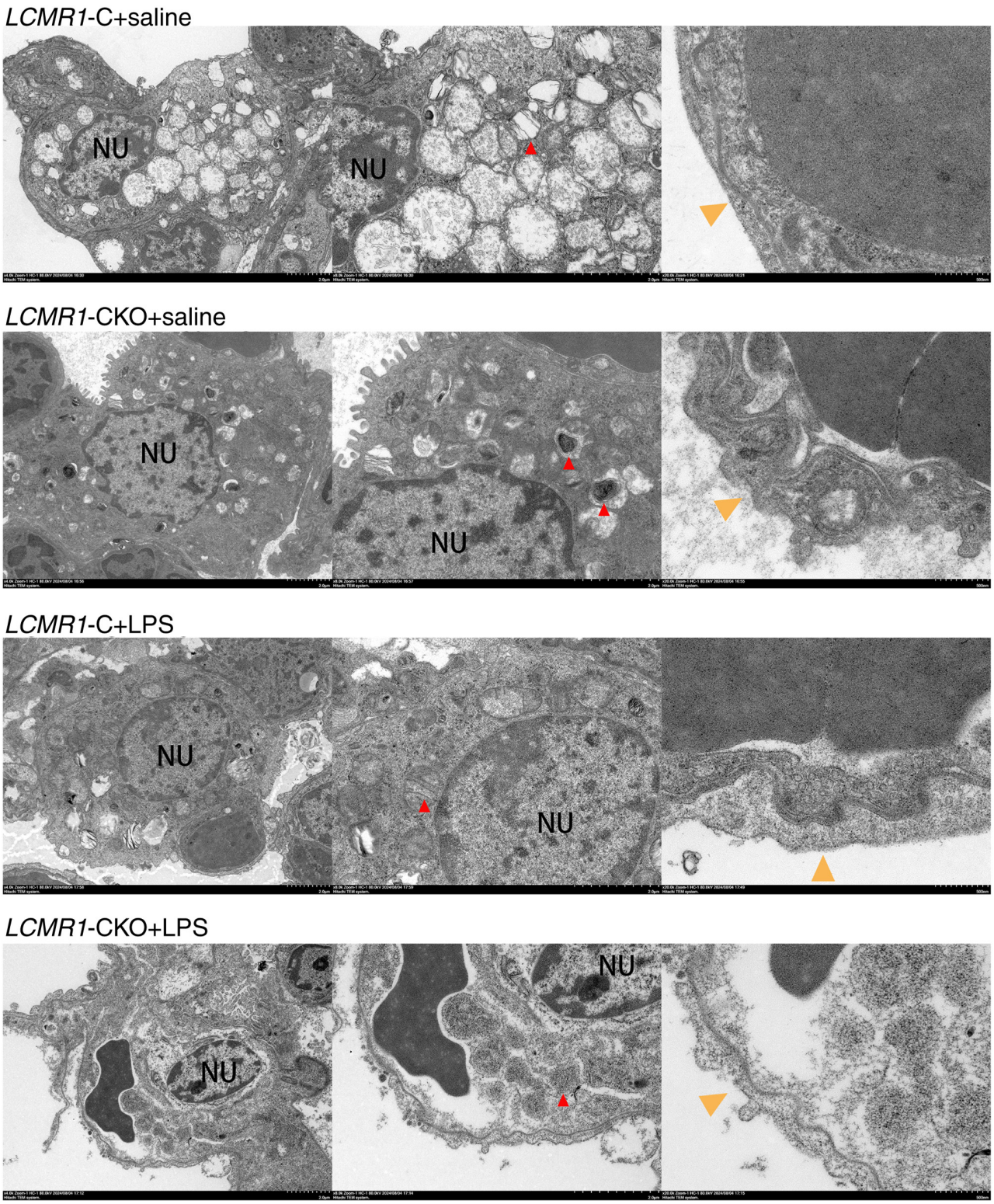

Figure 4. Representative transmission electron microscopy images of lung sections. Red arrows indicate lamellar bodies in type II alveolar epithelial cells; yellow arrows indicate the air-blood barrier. Scale bars: Left panels (2 μm, x4,000), right panels (500 nm, x20,000), middle panels (2 μm, x8,000). C, control; CKO, conditional knockout; *LCMR1*, lung cancer metastasis-related protein 1; LPS, lipopolysaccharide; NU, nucleus.

epithelial channal of the chips, but the results showed no statistical differences between the groups (Fig. 6G-J).

To further clarify the mechanism of air-blood barrier dysfunction caused by *LCMR1* deficiency, the possible molecular mechanisms involved were examined. The protein expression levels of apoptosis and differentiation-related molecules were examined in samples extracted from lung-on-a-chip models. The expression of AQP5, a marker of AEC-II differentiation into type I alveolar epithelial cells (AEC-I), was analyzed. After LPS stimulation, AQP5 expression was upregulated in *LCMR1*-OE chips compared with in LPS-induced HPAEpic chips, suggesting enhenced differentiation (Fig. 7A and B). However,

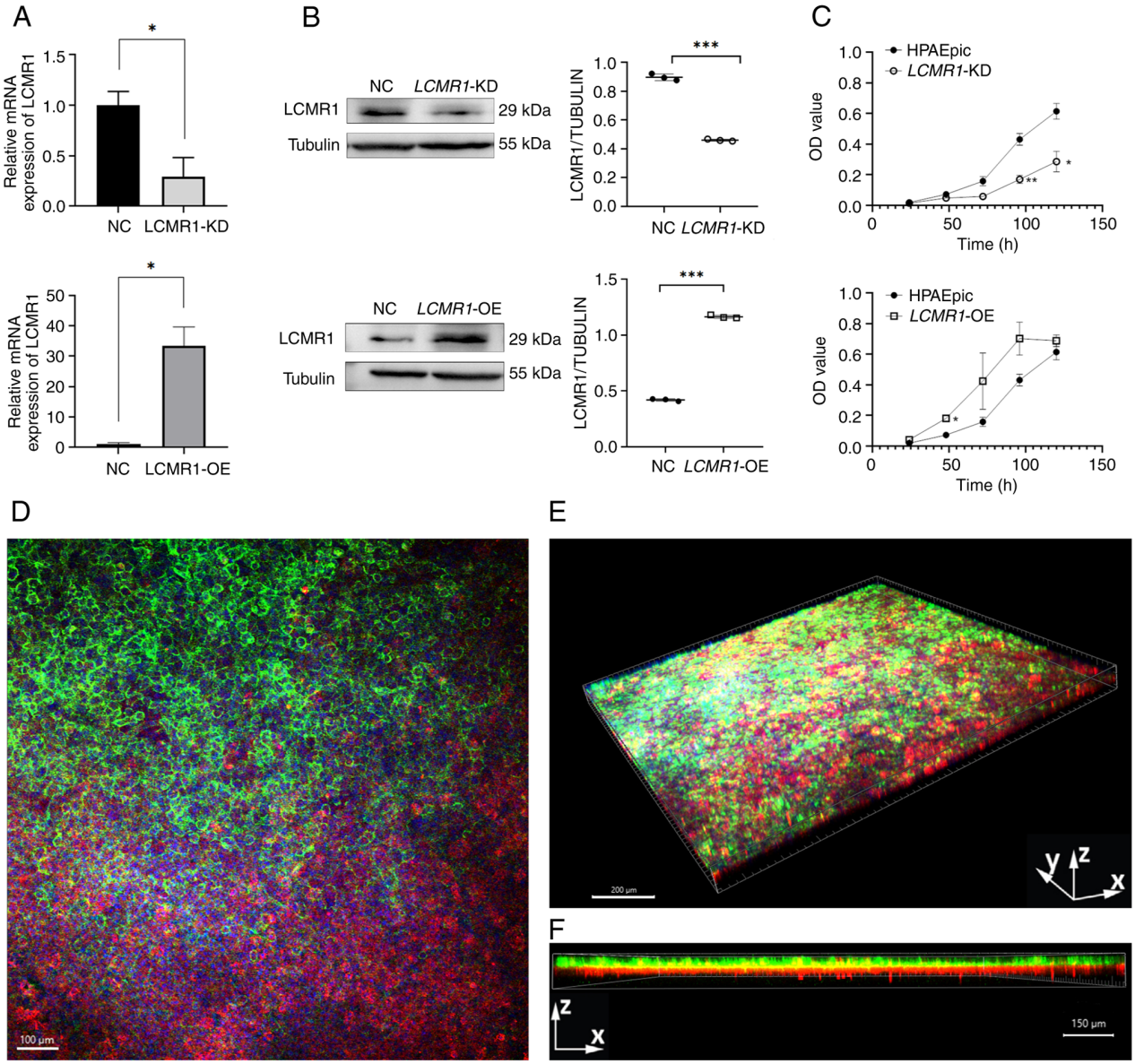

Figure 5. Generation of lung-on-a-chip model. (A) *LCMR1* mRNA expression in *LCMR1*-OE and *LCMR1*-KD cells, normalized to *β-actin*. (B) Western blot analysis of LCMR1 protein in *LCMR1*-OE cells and *LCMR1*-KD cells, ***P<0.0001 as determined by unpaired Student's t-test. (C) Proliferation rate of *LCMR1*-OE and *LCMR1*-KD cells. *P<0.05, **P<0.01 vs. HPAEpic. (D) 2D planar view of the lung-on-a-chip by confocal fluorescence microscopy. (E) Representative 3D reconstructed confocal image of the lung-on-a-chip; The epithelium was marked by E-cadherin, stained in red; the endothelium was marked by VE-cadherin, stained in green. (F) Image of the lung-on-a-chip from side view; the epithelium and endothelium formed a clear barrier. *LCMR1*, lung cancer metastasis-related protein 1; *LCMR1*-KD, *LCMR1*-knockdown; *LCMR1*-OE, *LCMR1*-overexpressing; NC, negative control.

compared with that in the HPAEpic chips, the protein expression levels of AQP5 in the *LCMR1*-KD chips were decreased after LPS stimulation, suggesting dysfunctional differentiation (Fig. 7A and C). Markers of apoptosis were also examined, and increased Bax/Bcl-2 and cleaved caspase-3/caspse-3 protein ratios were detected in the *LCMR1*-KD chips compared with HPAEpic chips, with or without LPS, suggesting increased apoptosis. The *LCMR1*-OE chips, however, showed no significant changes in Bax/Bcl-2 and cleaved caspase-3/caspse-3 protein ratios comparing to the HPAEpic chips (Fig. 7D-I).

Discussion

Since the discovery of the *LCMR1* gene in lung cancer, research on *LCMR1* has mainly focused on cancer; notably, a number of reports have shown that *LCMR1* serves an important role not only in lung cancer, but also in a variety of other types of cancer. Through large-scale RNA interference screening, Agaësse *et al* (29) identified *LCMR1* as a key regulator of melanoma invasion, and Wang *et al* (20) reported that *LCMR1* could promote the metastasis of advanced metastatic prostate cancer. However, the role of this gene in other diseases, particularly inflammatory diseases, has yet to be investigated. The present study, to the best of our knowledge, is the first to examine the role of this gene in noncancerous diseases.

In experiments using wild-type mice to construct an LPS-induced ALI model, 14) of mice died within 72 h after LPS injection, and the results presented in the current study are from mice that were still alive at each time point. Although

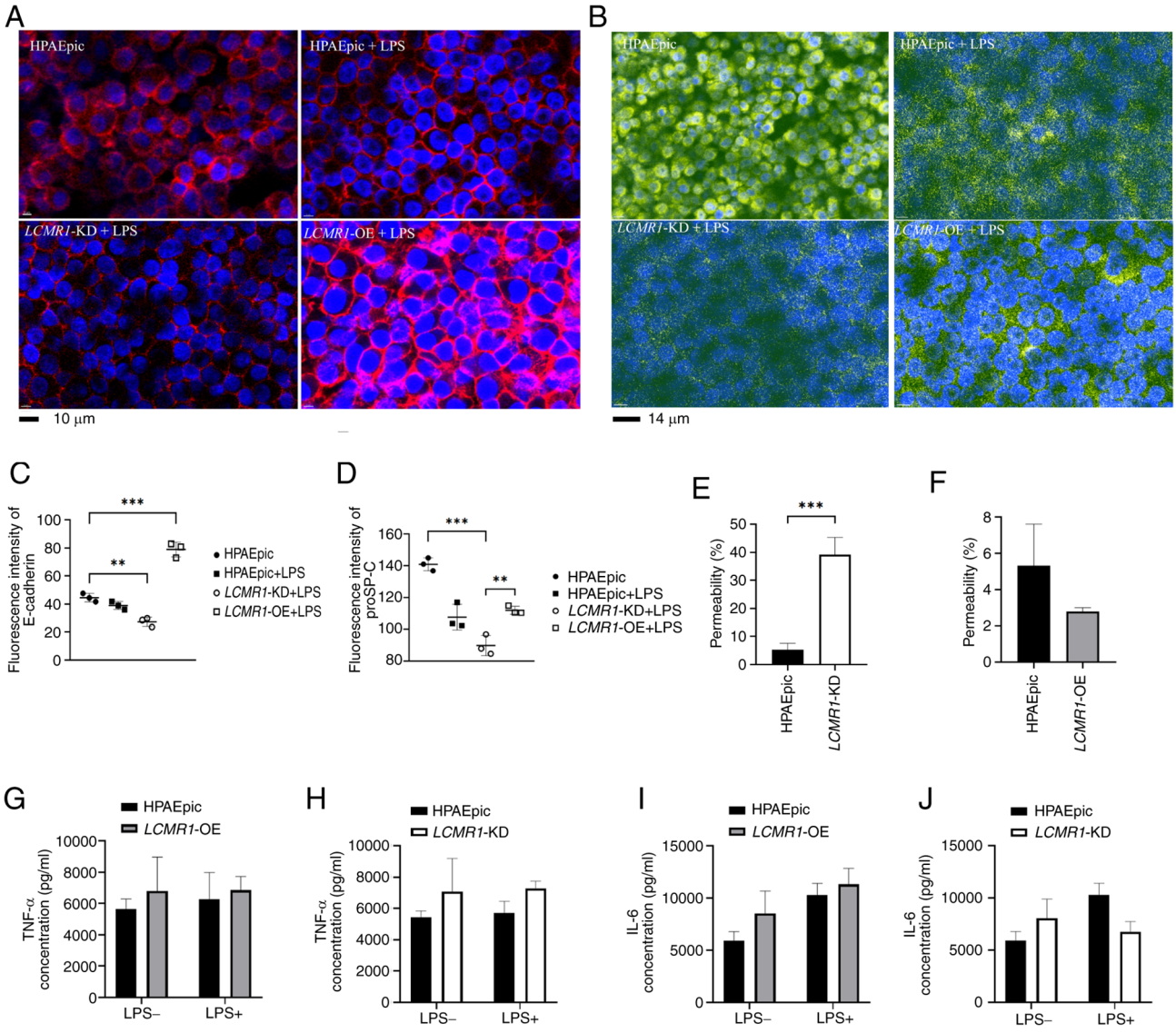

Figure 6. Knockdown of *LCMR1* impairs the structure and function of the air-blood barrier. (A) Immunofluorescence of E-cadherin in the epithelial cell layer of the lung-on-a-chip under different conditions. Red: E-cadherin; blue: DAPI. (B) Immunofluorescence of proSP-C in the epithelial cell layer of the chips under different conditions. Green: proSP-C; blue: DAPI. Comparison of the quantified immunofluorescence intensities of (C) E-cadherin and (D) proSP-C (n=3/group). **P<0.001, ***P<0.0001, as determined by one-way analysis of variance followed by Tukey's post hoc test. (E) Permeability rate of the *LCMR1*-KD chips comparing to HPAEpic chips calculated by comparing the fluorescence intensity of the epithelial channel and the vascular channel (n=3/group). ***P<0.0001. (F) Permeability rate of the *LCMR1*-OE chips comparing to HPAEpic chips calculated by comparing the fluorescence intensity of the epithelial channel and the vascular channel (n=3/group). (G and H) Concentration of TNF-α in the supernatant of chips (n=3/group). (I and J) Concentration of IL-6 in supernatant of chips (n=3/group). *LCMR1*, lung cancer metastasis-related protein 1; LPS, lipopolysaccharide; proSP-C, pro-pulmonary surfactant C.

these mice survived for >72 h, it does not mean that the lungs of these mice have returned to normal, and there may still be inflammatory infiltration and edema; a previous study reported that the inflammatory response peaked at ~2 days and returned to baseline at ~10 days after intratracheal LPS injection (30). The present study assessed the expression of LCMR1 from 0 to 96 h after LPS injection to clarify the change in LCMR1 expression after LPS-induced ALI. From the findings of LPS-induced ALI in wild-type mice, it was revealed that the expression of *LCMR1* was significantly decreased during the acute phase of LPS-induced lung injury (within 48 h after LPS challenge). However, the expression of *LCMR1* rebounded after 48 h (the acute phase). These results suggested that *LCMR1* may be involved in the repair of lung injury and could serve a protective role in the course of lung injury.

To further demonstrate the protective role of *LCMR1* in ALI, *LCMR1*-CKO mice were used to generate an LPS-induced ALI model. The results revealed that mice with conditional knockout of *LCMR1* in AEC-II presented with more severe lung function decline, lung inflammation and pathological damage after LPS challenge than the *LCMR1*-C mice and *LCMR1*-CKO mice without LPS administration. This finding is consistent with our previous study, which showed that mice developed lung injury at ~15 days after knockout (18). However, in the present study, LPS injection was performed 24 h after tamoxifen induction, and lungs were harvested 48 h after LPS administration (72 h after induced knockout). The timepoint is earlier than the time of phenotypic changes detected in mice in the previous study. At this timepoint, the results showed that the *LCMR1*-CKO mice given saline did not show significant pathological and

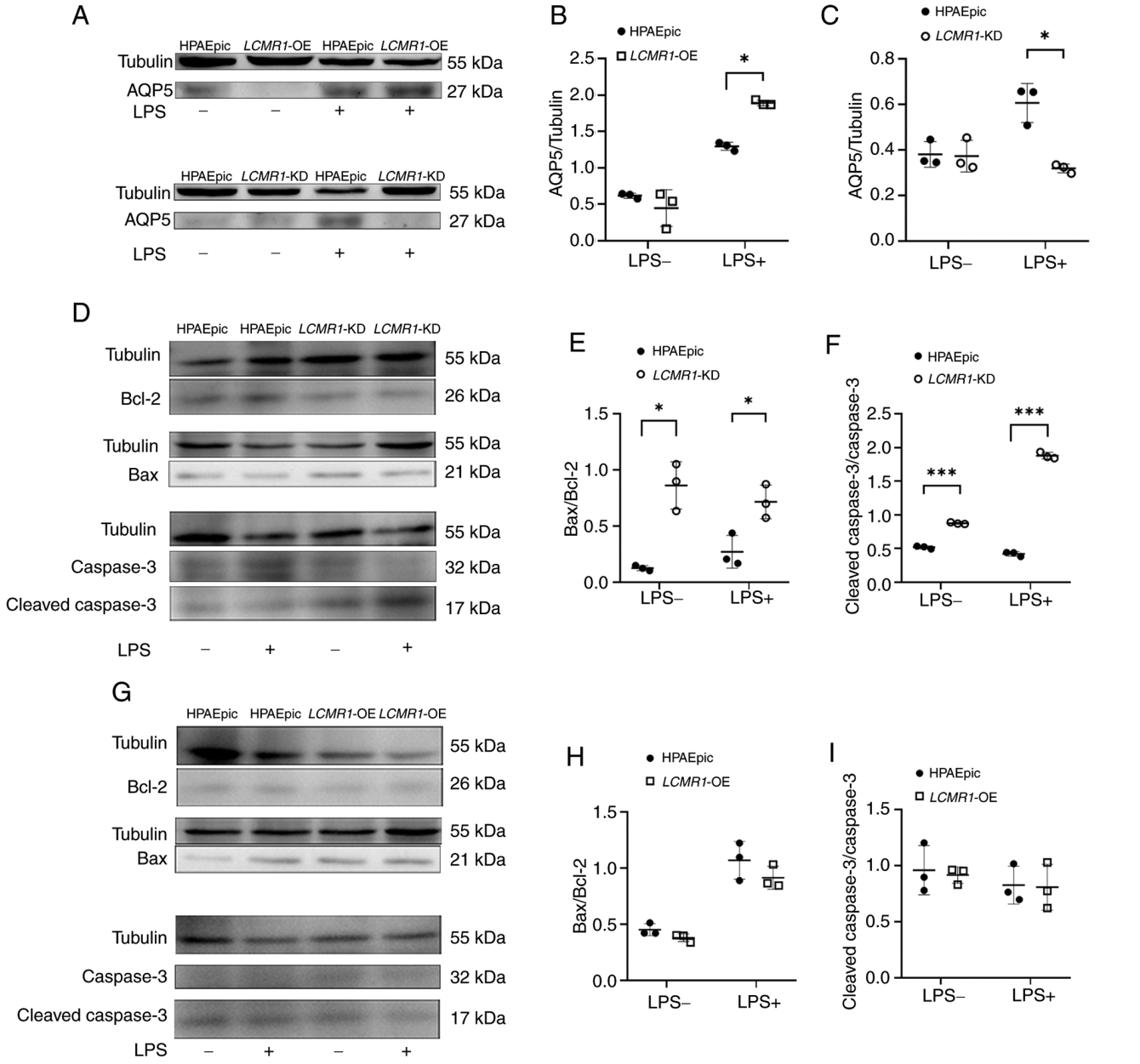

Figure 7. Air-blood barrier impairment after *LCMR1* knockdown may be associated with impaired differentiation and enhanced apoptosis. (A) Representative western blot image of AQP5 protein in *LCMR1*-OE and *LCMR1*-KD chips before and after LPS stimulation. (B) Gray value analysis of AQP5 protein expression of the *LCMR1*-OE chips comparing to the HPAEpic chips (n=3/group). *P<0.05, as determined by two-way analysis of variance followed by Sidak's post hoc test. (D) Representative western blot image of Bcl-2, Bax, cleaved caspase-3 and caspase-3 proteins in *LCMR1*-KD chips before and after LPS stimulation. (E) Gray-scale analysis of Bax/Bcl-2 ratio in *LCMR1*-KD chips (n=3). (F) Gray-scale analysis of cleaved caspase-3/caspase-3 ratio in *LCMR1*-KD chips (n=3). (G) Representative western blot image of Bcl-2, Bax, cleaved caspase-3 and caspase-3 protein in *LCMR1*-OE chips before and after LPS stimulation. (H) Gray-scale analysis of Bax/Bcl-2 ratio in *LCMR1*-OE chips (n=3). (I) Gray-scale analysis of cleaved caspase-3/caspase-3 ratio in *LCMR1*-OE chips (n=3). *P<0.05 and ***P<0.001, as determined by two-way analysis of variance followed by Sidak's post hoc test. AQP5, aquaporin 5; *LCMR1*, lung cancer metastasis-related protein 1; *LCMR1*-KD, *LCMR1*-knockdown; *LCMR1*-OE, *LCMR1*-overexpressing; LPS, lipopolysaccharide.

functional changes, whereas the *LCMR1*-CKO mice given LPS suffered significant lung injury, which suggested that *LCMR1* knockout aggravated the course of LPS-induced lung injury.

Destruction of AEC-II and damage to the air-blood barrier were observed by transmission electron microscopy, suggesting *LCMR1* may affect the homeostasis of the air-blood barrier. In order to clarify the effect of *LCMR1* on the alveolar air-blood barrier, organ-on-a-chip technology was applied. Organ-on-a-chip technology is an emerging method that combines bioengineering and material technology, and can reconstruct the microenvironment and microstructure of lung cells *in vitro*. Some studies have used organ-on-a-chip models to mimic lung diseases. Zhang *et al* used an alveolar-chip model to simulate the infection process of SARS-CoV-2, which greatly reduced the difficulty and cost of studying this pathogen (27). Dasgupta *et al* (31) constructed a lung-on-a-chip model of radiation-induced ALI; compared with the preclinical animal model, the radiation dose sensitivity observed on the chip was more similar to that of the human lung, and the effect of therapeutic drugs on radiation-induced ALI was intuitively

evaluated using this model. These findings indicated that lung-on-a-chip is an intuitive, visual and easy-to-control model, which can be used to simulate the microenvironment of various lung diseases. The current study used this model to more intuitively and conveniently reflect the effect of the *LCMR1* gene on lung injury. The present study revealed that knockdown of *LCMR1* resulted in impaired tight junctions in the alveolar epithelium and reduced expression of E-cadherin, indicating impaired air-blood barrier function and impaired barrier tightness as reflected by leakage of fluorescent substances. In addition, knockdown of *LCMR1* resulted in decrease in proSP-C in epithelial cells after LPS stimulation suggests a disorder of cellular synthetic function. As the proSP-C is a crucial alveolar surfactant which maintain alveolar pressure and preventing alveolar collapse (32), its reduction similarly affects air-blood barrier function. Notably, in the current study, LPS stimulation time on lung-on-a-chip model was 72 h, which is longer than previous cell-based studies. In cell-based studies, the duration of LPS stimulation has generally been reported to be <24 h (33,34). This may be similar to the *in vivo* environment, as the continuous flow of medium supplemented with LPS mimicking the real *in vivo* injury stimulus.

The *LCMR1* gene encodes a subunit of the cellular transcription mediator complex and is also known as MED19 (35). Mediator complexes are crucial in the proliferation and metastasis of malignant tumors as they modulate various signal transduction pathways associated with cell growth, differentiation, the cell cycle and apoptosis (35). After the expression of the *LCMR1* gene was altered by lentiviral infection in HPAEpiC cells, the proliferation rate of cells with overexpression of *LCMR1* accelerated, whereas the proliferation rate of cells with knockdown of *LCMR1* decreased, indicating that *LCMR1* may affect the proliferation of cells. This observation is consistent with the clinical manifestation that tumors with high expression of LCMR1 are more prone to metastasis (36,37). By contrast, the present results from the lung-on-a-chip model revealed that knockdown of the oncogene *LCMR1* increased the susceptibility of normal alveolar epithelial cells to lung injury. The decreased expression of E-cadherin suggested damage to epithelial tight junctions, whereas the decrease in proSP-C suggested a decrease in cell synthesis, all of which indicated that cell dysfunction may occur after knockdown of *LCMR1*. Different protein isoforms of LCMR1 have been reported to have different effects on gene expression (38). It could be hypothesized that LCMR1, which promotes metastasis in cancer, is a different isoform than LCMR1 that maintains cell homeostasis, and further studies are needed to clarify the specific mechanism of LCMR1 isoforms.

The mechanism of LPS-induced ALI also includes an increased inflammatory response. In the present study, mice with *LCMR1* conditional knockout in AEC-II exhibited a more severe inflammatory response, manifested by increased protein and inflammatory cytokine levels in the BALF. However, there was no significant change in inflammatory cytokine levels in the lung-on-a-chip model. It could be hypothesized that this may be due to the absence of immune cells in the lung-on-a-chip model. In a study of SARS-CoV-2 infection on a lung-on-a-chip model, more severe epithelial damage and elevated inflammatory cytokines were observed after the addition of circulating immune cells (27). A similar result has been observed in a lung-on-a-chip model of radiation-induced ALI; the presence of peripheral blood mononuclear cells at the time of radiation exposure was shown to lead to a persistent and progressive inflammatory response in the chips (31). The different results between the *in vivo* and lung-on-a-chip models in the present study may be related to this. The enhanced inflammatory response *in vivo* may be a secondary result of the infiltration of inflammatory cells after the impairment of the lung air-blood barrier caused by *LCMR1* knockdown.

The present study demonstrated that the knockdown of *LCMR1* could potentially disrupt cellular differentiation processes. Following induction with LPS, the expression levels of AQP5 in the *LCMR1*-KD chips were diminished in comparison with the control and *LCMR1*-OE chips. AQP5 is a marker of AEC-I. AEC-II serve a stem cell-like role in the lung and can differentiate into AEC-I during lung injury to have a role in repair (39). The present results suggested that knockdown of *LCMR1* may lead to impaired differentiation and impaired epithelial repair, which in turn aggravates injury. A similar phenomenon has been reported in a *P53* gene study; the p53 protein was shown to promote alveolar regeneration following ALI by boosting the self-renewal of AEC-II and facilitating their differentiation into mature AEC-I (40). Taken together, these results suggested the potential protective role of oncogenes in inflammatory diseases such as ALI, and may provide new targets for the prevention and treatment of these diseases.

Knockout of *LCMR1* may also aggravate lung injury through enhanced apoptosis. In the present study, both lung-on-a-chip and animal models showed an increase in the expression ratio of Bax/Bcl-2 after knockdown or knockout of *LCMR1*, suggesting enhanced apoptosis. This is similar to the results of some previous studies on tumors. Xu *et al* (41) reported that the interaction between LCMR1 and DEK can synergistically inhibit the apoptosis of lung cancer cells, and this effect may be related to the induction of the myeloid leukemia protein cell differentiation protein 1 pathway. Zhang *et al* (42) reported that miroRNA-4778-3p can specifically bind to LCMR1 and negatively regulate its expression, which eventually leads to the downregulation of the expression of the apoptosis-related molecules caspase-3, caspase-8 and caspase-9. Notably, in the *LCMR1*-OE chip findings in the present study, there was no significant difference in apoptotic proteins compared with the control group. It could be hypothesized that overexpression of *LCMR1* inhibited apoptosis to a certain extent, so that the apoptosis protein level was not significantly increased even in the presence of LPS. Future studies should investigate the relationship between LCMR1 and apoptosis, particularly the relevant mechanism in the case of *LCMR1* overexpression.

In conclusion, the present study indicated that *LCMR1* deficiency aggravated LPS-induced ALI in an animal model and a lung-on-a-chip model. To the best of our knowledge, the present study is the first regarding the function of this oncogene in diseases other than cancer, which suggested that *LCMR1* may serve a phylactic role in ALI by affecting the apoptosis and differentiation of AEC-II. *LCMR1* could contribute to the process of inflammatory diseases such as ALI and may therefore be considered a new therapeutic target. The present study also demonstrated the possibility of using organ-on-chip

technology for gene editing research, which may make it more convenient, intuitive and economical to study the function of specific genes in the future.

The present study has some limitations. First, due to the reduced lifespan of *LCMR1*-CKO mice, long-term observation data were not acquired. Second, the specific pathways and mechanism of *LCMR1* have not been well studied. In future studies, we aim to further clarify the in-depth mechanism based on transcriptome sequencing data from *LCMR1*-OE and *LCMR1*-KD lung-on-a-chip samples.

Acknowledgements

The authors would like to thank Professor Jianhua Qin (Division of Biotechnology, CAS Key Laboratory of SSAC, Dalian Institute of Chemical Physics, Chinese Academy of Sciences) and their team for technical assistance.

Funding

No funding was received.

Availability of data and materials

The data generated in this study are available on request from the corresponding author.

Author's contributions

ZM, XM and LC conceived and designed the study, ZM and XM conducted the experiments, and drafted and revised the manuscript. CS, JL, JR, LL, YW and YL participated in cell and animal experiments. CL and ZY analyzed data. All authors read and approved the final version of the manuscript. ZM, XM and LC confirm the authenticity of all the raw data.

Ethics approval and consent to participate

The experimental protocol was approved by the Animal Ethics Committee of Chinese PLA General Hospital (approval no. SQ2023672; Beijing, China).

Patient consent for publication

Not applicable.

Competing interests

The authors declare that they have no competing interests.

References

1. Long ME, Mallampalli RK and Horowitz JC: Pathogenesis of pneumonia and acute lung injury. Clin Sci (Lond) 136: 747-769, 2022.
2. Wick KD, Ware LB and Matthay MA: Acute respiratory distress syndrome. BMJ 387: e076612, 2024.
3. Bellani G, Laffey JG, Pham T, Fan E, Brochard L, Esteban A, Gattinoni L, van Haren F, Larsson A, McAuley DF, *et al*: Epidemiology, patterns of care, and mortality for patients with acute respiratory distress syndrome in intensive care units in 50 countries. JAMA 315: 788-800, 2016.
4. Liu H, Yu X, Yu S and Kou J: Molecular mechanisms in lipopolysaccharide-induced pulmonary endothelial barrier dysfunction. Int Immunopharmacol 29: 937-946, 2015.
5. Bos LDJ and Ware LB: Acute respiratory distress syndrome: Causes, pathophysiology, and phenotypes. Lancet 400: 1145-1156, 2022.
6. Wang Y, Wang L, Ma S, Cheng L and Yu G: Repair and regeneration of the alveolar epithelium in lung injury. FASEB J 38: e23612, 2024.
7. Woods SJ, Waite AA, O'Dea KP, Halford P, Takata M and Wilson MR: Kinetic profiling of in vivo lung cellular inflammatory responses to mechanical ventilation. Am J Physiol Lung Cell Mol Physiol 308: L912-L921, 2015.
8. Li N, Liu B, Xiong R, Li G, Wang B and Geng Q: HDAC3 deficiency protects against acute lung injury by maintaining epithelial barrier integrity through preserving mitochondrial quality control. Redox Biol 63: 102746, 2023.
9. Chen H, Lin X, Yi X, Liu X, Yu R, Fan W, Ling Y, Liu Y and Xie W: SIRT1-mediated p53 deacetylation inhibits ferroptosis and alleviates heat stress-induced lung epithelial cells injury. Int J Hyperthermia 39: 977-986, 2022.
10. Hiemstra PS, Tetley TD and Janes SM: Airway and alveolar epithelial cells in culture. Eur Respir J 54: 1900742, 2019.
11. Perelson AS and Ribeiro RM: Introduction to modeling viral infections and immunity. Immunol Rev 285: 5-8, 2018.
12. Ma C, Peng Y, Li H and Chen W: Organ-on-a-Chip: A new paradigm for drug development. Trends Pharmacol Sci 42: 119-133, 2021.
13. Tan J, Guo Q, Tian L, Pei Z, Li D, Wu M, Zhang J and Gao X: Biomimetic lung-on-a-chip to model virus infection and drug evaluation. Eur J Pharm Sci 180: 106329, 2023.
14. Bai H, Si L, Jiang A, Belgur C, Zhai Y, Plebani R, Oh CY, Rodas M, Patil A, Nurani A, *et al*: Mechanical control of innate immune responses against viral infection revealed in a human lung alveolus chip. Nat Commun 13: 1928, 2022.
15. Nawroth JC, Lucchesi C, Cheng D, Shukla A, Ngyuen J, Shroff T, Varone A, Karalis K, Lee HH, Alves S, *et al*: A microengineered airway lung chip models key features of Viral-induced exacerbation of asthma. Am J Respir Cell Mol Biol 63: 591-600, 2020.
16. Wang P, Jin L, Zhang M, Wu Y, Duan Z, Guo Y, Wang C, Guo Y, Chen W, Liao Z, *et al*: Blood-brain barrier injury and neuroinflammation induced by SARS-CoV-2 in a lung-brain microphysiological system. Nat Biomed Eng 8: 1053-1068.
17. Chen L, Liang Z, Tian Q, Li C, Ma X, Zhang Y, Yang Z, Wang P and Li Y: Overexpression of LCMR1 is significantly associated with clinical stage in human NSCLC. J Exp Clin Cancer Res 30: 18, 2011.
18. Wang Y, Li C, Wu Z, Dai Y, Liu L and Chen L: Deletion of LCMR1 in alveolar type II cells induces lethal impairment of lung structure and function in adult mice. J Thorac Dis 15: 1445-1459, 2023.
19. Bao X, Zhao L, Guan H and Li F: Inhibition of LCMR1 and ATG12 by demethylation-activated miR-570-3p is involved in the anti-metastasis effects of metformin on human osteosarcoma. Cell Death Dis 9: 611, 2018.
20. Wang K, Wang X, Fu X, Sun J, Zhao L, He H and Fan Y: Lung cancer metastasis-related protein 1 promotes the transferring from advanced metastatic prostate cancer to castration-resistant prostate cancer by activating the glucocorticoid receptor alpha signal pathway. Bioengineered 13: 5373-5385, 2022.
21. Liu L, Li C, Wu Z, Li Y, Yu H, Li T, Wang Y, Zhao W and Chen L: LCMR1 promotes Large-cell lung cancer proliferation and metastasis by downregulating HLA-Encoding genes. Cancers (Basel) 15: 5445, 2023.
22. Percie du Sert N, Hurst V, Ahluwalia A, Alam S, Avey MT, Baker M, Browne WJ, Clark A, Cuthill IC, Dirnagl U, *et al*: The ARRIVE guidelines 2.0: Updated guidelines for reporting animal research. PLoS Biol 18: e3000410, 2020.
23. Shrum B, Anantha RV, Xu SX, Donnelly M, Haeryfar SM, McCormick JK and Mele T: A robust scoring system to evaluate sepsis severity in an animal model. BMC Res Notes 7: 233, 2014.
24. Stanojevic S, Kaminsky DA, Miller MR, Thompson B, Aliverti A, Barjaktarevic I, Cooper BG, Culver B, Derom E, Hall GL, *et al*: ERS/ATS technical standard on interpretive strategies for routine lung function tests. Eur Respir J 60: 2101499, 2022.
25. Glaab T, Taube C, Braun A and Mitzner W: Invasive and noninvasive methods for studying pulmonary function in mice. Respir Res 8: 63, 2007.
26. Fukumoto J, Fukumoto I, Parthasarathy PT, Cox R, Huynh B, Ramanathan GK, Venugopal RB, Allen-Gipson DS, Lockey RF and Kolliputi N: NLRP3 deletion protects from hyperoxia-induced acute lung injury. Am J Physiol Cell Physiol 305: C182-C189, 2013.

27. Zhang M, Wang P, Luo R, Wang Y, Li Z, Guo Y, Yao Y, Li M, Tao T, Chen W, *et al*: Biomimetic human disease model of SARS-CoV-2-Induced lung injury and immune responses on organ chip system. Adv Sci (Weinh) 8: 2002928, 2021.
28. Livak KJ and Schmittgen TD: Analysis of relative gene expression data using real-time quantitative PCR and the 2(-Delta Delta C(T)) method. Methods 25: 402-408, 2001.
29. Agaesse G, Barbollat-Boutrand L, Sulpice E, Bhajun R, El Kharbili M, Berthier-Vergnes O, Degoul F, de la Fouchardière A, Berger E, Voeltzel T, *et al*: A large-scale RNAi screen identifies LCMR1 as a critical regulator of Tspan8-mediated melanoma invasion. Oncogene 36: 5084, 2017.
30. Wang L, Wang X, Tong L, Wang J, Dou M, Ji S, Bi J, Chen C, Yang D, He H, *et al*: Recovery from acute lung injury can be regulated via modulation of regulatory T cells and Th17 cells. Scand J Immunol 88: e12715, 2018.
31. Dasgupta Q, Jiang A, Wen AM, Mannix RJ, Man Y, Hall S, Javorsky E and Ingber DE: A human lung alveolus-on-a-chip model of acute radiation-induced lung injury. Nat Commun 14: 6506, 2023.
32. Sehlmeyer K, Ruwisch J, Roldan N and Lopez-Rodriguez E: Alveolar dynamics and Beyond-The importance of surfactant protein C and cholesterol in lung homeostasis and fibrosis. Front Physiol 11: 386, 2020.
33. Xiao K, He W, Guan W, Hou F, Yan P, Xu J, Zhou T, Liu Y and Xie L: Mesenchymal stem cells reverse EMT process through blocking the activation of NF-κB and Hedgehog pathways in LPS-induced acute lung injury. Cell Death Dis 11: 863, 2020.
34. Li J, Deng SH, Li J, Li L, Zhang F, Zou Y, Wu DM and Xu Y: Obacunone alleviates ferroptosis during lipopolysaccharide-induced acute lung injury by upregulating Nrf2-dependent antioxidant responses. Cell Mol Biol Lett 27: 29, 2022.
35. Zhang Y, Qin P, Tian L, Yan J and Zhou Y: The role of mediator complex subunit 19 in human diseases. Exp Biol Med (Maywood) 246: 1681-1687, 2021.
36. Zhang X, Fan Y, Liu B, Qi X, Guo Z and Li L: Med19 promotes breast cancer cell proliferation by regulating CBFA2T3/HEB expression. Breast Cancer 24: 433-441, 2017.
37. Zhang X, Gao D, Fang K, Guo Z and Li L: Med19 is targeted by miR-101-3p/miR-422a and promotes breast cancer progression by regulating the EGFR/MEK/ERK signaling pathway. Cancer Lett 444: 105-115, 2019.
38. Ruoff R, Weber H, Wang Y, Huang H, Shapiro E, Fenyo D and Garabedian MJ: MED19 encodes two unique protein isoforms that confer prostate cancer growth under low androgen through distinct gene expression programs. Sci Rep 13: 18227, 2023.
39. Liu K, Meng X, Liu Z, Tang M, Lv Z, Huang X, Jin H, Han X, Liu X, Pu W, *et al*: Tracing the origin of alveolar stem cells in lung repair and regeneration. Cell 187: 2428-2445.e20, 2024.
40. Kaiser AM, Gatto A, Hanson KJ, Zhao RL, Raj N, Ozawa MG, Seoane JA, Bieging-Rolett KT, Wang M, Li I, *et al*: p53 governs an AT1 differentiation programme in lung cancer suppression. Nature 619: 851-859, 2023.
41. Xu Y, Liang Z, Li C, Yang Z and Chen L: LCMR1 interacts with DEK to suppress apoptosis in lung cancer cells. Mol Med Rep 16: 4159-4164, 2017.
42. Zhang Y, Li P, Hu J, Zhao LN, Li JP, Ma R, Li WW, Shi M and Wei LC: Role and mechanism of miR-4778-3p and its targets NR2C2 and Med19 in cervical cancer radioresistance. Biochem Biophys Res Commun 508: 210-216, 2019.